# Microscopic calculations of effective charges and quadrupole transition rates in Si, S and Ar isotopes.

**R. A. Radhi, A. H. Ali\***

Department of Physics, College of Science, University of Baghdad, Baghdad, Iraq

**Abstract.**

Quadrupole transition rates and effective charges are calculated for even-even Si, S and Ar isotopes based on *sd* and *sdpf* -shell model spaces. Shell model calculations are performed with *sd* shell-model space for neutron number ($N$) $\leq 20$ and *sdpf* shell-model space for N > 20. Excitation out of major shell space are taken into account through a microscopic theory which allows particle-hole excitation from the core and model space orbits to all higher orbits with $2\hbar\omega$ excitation. Effective charges are obtained for each isotope. The results show a systematic increase in the $B(E2)$ values for $N \geq 20$. Shell model calculation predicts the erosion of the $N$=28 magicity in the neutron rich [42]Si. No clear indications about the erosion of the shell gap closure in [44]S and [46]Ar isotope.

**Keywords:** Shell models calculations; Effective charges; Quadrupole transition rates.

حسابات مجهرية للشحنات الفعالة و معدلات الانتقال الرباعية في نظائر سيلكون،الكبريت والااركون

**رعد عبدالكريم راضي ،احمد حسين علي\***

قسم الفيزياء ، كلية العلوم ، جامعة بغداد ، بغداد ، العراق

**الخلاصة:**

حسبت معدلات الانتقال الرباعية القطب والشحنات الفعالة لنظائر نوى زوجي- زوجي السيلكون ،الكبريت والااركون على اساس نموذج فضاءات قشرة *sd* و *sdpf* . نفذت العمليات الحسابية بنموذج فضاء القشرة *sd* لعدد نيوترونات اصغر اويساوي 20 وفضاء نموذج القشرة *sdpf* لعدد نيوترونات اكبر من 20 . يتم الاخذ في الحسبان التهيجات خارج فضاء القشرة الرئيسية من خلال النظرية المايكروية (المجهرية) التي تسمح تهيج جسيم- فجوه (particle-hole) من مدارات القلب و مدارات التكافؤ الى المدارات ألاعلى بتهيج $2\hbar\omega$. أظهرت النتائج زيادة منتظمة في قيم الانتقالات رباعية القطب لعدد نيوترونات اكبر او يساوي 20. توقعات حساب نموذج القشرة هي انعدام العدد السحري $N$=28 في Si [42] الغني بالنيوترونات . لا مؤشرات واضحة حول انعدام فجوة القشرة في نظير S[44] ونظير Ar [46] .

## 1. Introduction

Neutron-rich nuclei far from stability line provide an attractive testing ground of nuclear structure studies. They have been extensively investigated because their exotic properties which are different from those of stable nuclei. In the last two decades, development of experiments with a secondary radioactive ion beam has extensively helped the studies on light neutron-rich nuclei. One of the most striking features in neutron-rich nuclei is the nuclear deformation. The deformation can be investigated experimentally and theoretically, through their electromagnetic transitions. The general trend of the $2^+$ excitation energy $E_x(2_1^+)$ and the reduced electric quadrupole transition strength $B(E2;0_1^+ \to 2_1^+)$ for even-even nuclei are expected to be inversely proportional to one another [1]. Recent theoretical

_____

\*Email: ah70med15@gmail.com

studies and experimental data have questioned the persistence of the traditional magic numbers, and revealed that the $N = 28$ shell gap is eroded when moving away from the stability line. The experimental data for the $^{44}$S and $^{42}$Si isotones indicate a clear breaking of the $N = 28$ magicity because of the observed small $2^+$ energy [2–4]. It is now established that the shell gaps in nuclei evolve with the proton and/or neutron degrees of freedom, leading to vanishing shell closures or appearance of new magic numbers. Measurements of the energy of the first $2^+$ state, $E_x (2^+)$ and the absolute $B(E2; 0_1^+ \rightarrow 2_1^+)$ quadrupole excitation strength provide the necessary information about the persistence or break down of the shell gab. Coulomb excitation measurements [5] showed that $^{40;42;44}$S are collective with high $B(E2)$ values. Lifetimes of low-lying excited states of the neutron-rich $^{44,46}$Ar nuclei have been measured by Mangoni et al. [6], which show the increase in the deduced $B(E2)$ transition probability from $^{44}$Ar to the closed-shell nucleus $^{46}$Ar which contradicts the earlier results of Coulomb-excitation experiments [3,7]. Shell-model calculations using the standard effective charges $e_\pi = 1.5e$ and $e_v = 0.5e$ have been used [6] which agree with their measured values. Kaneko et al. [8] calculated the $B(E2)$ values of even-even neutron rich Si, S and Ar isotopes, using the monopole interaction (EPQQM) in the *sdpf* valence space. In their calculation, they adopted the effective charges $e_\pi = 1.15e$ and $e_v = 0.15e$ for Si isotope $e_\pi = 1.35e$ and ev = 0.35e for S isotopes and $e_\pi = 1.5e$ and $e_v = 0.5e$ for Ar isotopes. The quadrupole vibrational modes of neutron-rich $N=28$ isotones ($^{48}$Ca, $^{46}$Ar, $^{44}$S and $^{42}$Si) were investigated by using the canonical-bases time-dependent Hartree-Foch-Bogoliubov theory [9]. Nuclear mass measurements of $^{48}$Ar and $^{49}$Ar [10] provide strong evidence for the closed shell nature of neutron number $N= 28$ in argon, which is therefore the lowest even-Z element exhibiting the $N= 28$ closed shell.

Shell model within a restricted model space is not appropriate to describe $E2$ moments and transitions for stable nuclei. The electromagnetic properties can be supplemented to the usual shell model treatment by allowing excitation from the core and model space orbits into higher orbits. A perturbative theory treatment was made of core-polarization effects in electromagnetic and inelastic electron scattering transitions due to high-lying collective excitation, which showed that there was a natural disparity in neutron and proton polarizations [11]. The conventional approach to supplying this added ingredient to shell model wave functions is to redefine the properties of the valence nucleons from those exhibited by actual nucleons in free space to model-effective values [12]. Effective charges are introduced for evaluating $E2$ transitions in shell-model studies to take into account effects of model-space truncation. A systematic analysis has been made for observed $B(E2)$ values with shell-model wave functions using a least-squares fit with two free parameters gave standard proton and neutron effective charges, $e_\pi = 1.3e$ and $e_v = 0.5e$ [13], in *sd*-shell nuclei. It was well established that the $B(E2)$ values which are obtained in the *sd* model space calculations and the associated $C2$ form factors through the first maximum, are too small by about a factor of 3 [14]. The primary reason for this is that the "giant resonance' excitation operators coupled coherently with low lying states. Joseph et al. [15] discussed the reliability of the determination of neutron and proton effective charges in nuclear collective models from experimental effective neutron and proton matrix elements of the $0^+$ to $2^+$ transitions. Effective charge models were presented for ground states of odd-even and doubly odd nuclei and for $J^\pi = 2^+$ first excited states of doubly even *sd*-shell nuclei, to calculate the qudrupole moments of $A=17$-$39$ nuclei [16]. A two parameter least-square fit of the shell model densities to the $E2$ of $A=17$-$39$ nuclei yielded values of $e_\pi = 1.29e$ and $e_v = 0.49e$ [17]. The least-square fit for the effective charges $e_\pi = 1.36(5)e$ and $e_v = 0.45(5)e$ were used to calculate $M1$ and $E2$ moments and transition matrix elements, Gamow-Teller $\beta$-decay matrix elements, and spectroscopic factors for *sd*-shell nuclei from $A = 17$ to $A = 39$ [18]. The role of the core and the truncated space can be taken into consideration through a microscopic theory, which allows one particle–one hole ($1p$–$1h$) excitation of the core and also of the model space to describe these $E2$ properties. These effects provide a more practical alternative for calculating nuclear collectivity. These effects are essential in describing transitions involving collective modes such as $E2$ transition between states in the ground-state rotational band, such as in $^{18}$O [19].

In the present work, we will adopt shell model with harmonic oscillator (HO) single particle wave functions to calculate the $E2$ transition rates of even-even Si, S and Ar isotopes. The *sd* model space will be used for neutron number $N \leq 20$, which covered the orbits $1d_{5/2}$, $2s_{1/2}$ and $1d_{3/2}$ and *sdpf* model

space for *N* > 20 with full *sd* valence space for *Z*-8 protons and full *fp* valence space for *N*-20 neutrons.

One particle- one hole (1p–1h) excitation from the core and model space will be taken into consideration through first-order perturbation theory. These 1*p*–1*h* excitation from the core and model space orbits are considered into all higher allowed orbits with $2\hbar\omega$ excitation. Excitation up to $2\hbar\omega$ are found to be enough for sufficient convergence. These excitations are essential in obtaining a reasonable description of the data.

## 2. Theory

The one-body electric multipole transition operator with multipolarity *J* for a nucleon is given by [20]

$$\hat{O}_{JM}(\vec{r})_k = r_k^J Y_{JM}(\Omega_k),$$ (1)

The reduced electric matrix element between the initial and final states is

$$M(EJ) = \left\langle J_f \| \sum_k e(k)\hat{O}_J(\vec{r})_k \| J_i \right\rangle$$ (2)

where *k* is the electric charge for the *k*-th nucleon. Since *e*(*k*)= 0 for neutron, there should appear no direct contribution from neutrons; however, this point requires further attention: The addition of a valence neutron will induce polarization of the core into configurations outside the adopted model space. Such core polarization effect is included through perturbation theory which gives effective charges for the proton and neutron. The reduced electric matrix element can be written in terms of the proton and neutron contributions

$$M(EJ) = \sum_{t_z} e(t_z)\left\langle J_f \| \hat{O}_J(\vec{r},t_z) \| J_i \right\rangle,$$ (3)

where $t_z$ = 1/2 for a proton and $t_z$ = -1/2 for a neutron and $\left\langle J_f \| O_J(\vec{r},t_z) \| J_i \right\rangle$ which is expressed as the sum of the products of the one-body density matrix (OBDM) times the single-particle matrix elements,

$$\left\langle J_f \| \hat{O}_J(\vec{r},t_z) \| J_i \right\rangle = \sum_{jj'} OBDM(J_i,J_f,J,t_z,j,j')\left\langle j \| \hat{O}_J(\vec{r},t_z) \| j' \right\rangle,$$ (4)

where *j* and *j'* label single-particle states for the shell model space.

The role of the core and the truncated space can be taken into consideration through a microscopic theory, which combines shell model wave functions and configurations with higher energy as first order perturbation to describe *EJ* excitation: these are called core polarization effects. The reduced matrix elements of the electron scattering operator is expressed as a sum of the model space (MS) contribution and the core polarization (CP) contribution, as follows:

$$M(EJ) = \sum_{t_z}\left[e(t_z)\left\langle J_f \| \hat{O}_J(\vec{r},t_z) \| J_i \right\rangle_{MS} + e\left\langle J_f \| \Delta\hat{O}_J(\vec{r},t_z) \| J_i \right\rangle_{CP}\right]$$ (5)

Similarly, the CP electric matrix element is expressed as the sum of the products of the one-body density matrix (OBDM) times the single-particle matrix elements,

$$\left\langle J_f \| \Delta\hat{O}_J(\vec{r},t_z) \| J_i \right\rangle = \sum_{jj'} OBDM(J_i,J_f,J,t_z,j,j')\left\langle j \| \Delta\hat{O}_J(\vec{r},t_z) \| j' \right\rangle$$ (6)

The single- particle matrix element of the CP term is

$$\left\langle j \| \Delta\hat{O}_J \| j' \right\rangle = \left\langle j \| \hat{O}_J \frac{\hat{Q}}{E_i - H_0} V_{res} \| j' \right\rangle + \left\langle j \| V_{res} \frac{\hat{Q}}{E_f - H_0} \hat{O}_J \| j' \right\rangle$$

(7)

where the operator $\hat{Q}$ is the projection operator onto the space outside the model space. The single particle core-polarization terms given in equation (7) are written as [20]

$$\left\langle j \| \Delta\hat{O}_J \| j' \right\rangle = \sum_{j_1 j_2 \lambda} \frac{(-1)^{j'+j_2+\lambda}}{\varepsilon_{j'} - \varepsilon_j - \varepsilon_{j_1} + \varepsilon_{j_2}} (2\lambda+1)\begin{Bmatrix} j & j' & J \\ j_2 & j_1 & \lambda \end{Bmatrix}\sqrt{(1+\delta_{j_1 j})(1+\delta_{j_2 j'})}$$

$$\times \left\langle jj_1 | V_{res} | j'j_2 \right\rangle_\lambda \left\langle j_2 \| \hat{O}_J \| j_1 \right\rangle$$ (8)

+terms with $j_1$ and $j_2$ exchanged with an overall minus sign,

where the index $j_1$ runs over particle states and $j_2$ over hole states and $\varepsilon$ is the single-particle energy.

For the residual two-body interaction $V_{res}$, the two-body Michigan three range Yukawa (M3Y) interaction of Bertsch *et al.* [21] is adopted.

The electric matrix element can be represented in terms of only the model space matrix elements by assigning effective charges( $e^{\text{eff}}(t_z)$ ) to the protons and neutrons which are active in the model space,

$$M(EJ) = \sum_{t_z} e^{\text{eff}}(t_z) \left\langle J_f \| \hat{O}_J(\vec{r}, t_z) \| J_i \right\rangle_{MS} \tag{9}$$

The effective nucleon charge can be obtained as follows

$$e^{\text{eff}}(t_z) \left\langle J_f \| \hat{O}_J(\vec{r}, t_z) \| J_i \right\rangle_{MS} = e(t_z) \left\langle J_f \| \hat{O}_J(\vec{r}, t_z) \| J_i \right\rangle_{MS} + e \left\langle J_f \| \Delta\hat{O}_J(\vec{r}, t_z) \| J_i \right\rangle_{CP} \tag{10}$$

$$e^{\text{eff}}(t_z) = e(t_z) + \frac{\left\langle J_f \| \Delta\hat{O}_J(\vec{r}, t_z) \| J_i \right\rangle_{CP}}{\left\langle J_f \| \hat{O}_J(\vec{r}, t_z) \| J_i \right\rangle_{MS}} e = e(t_z) + e\delta e(t_z) \tag{11}$$

where $\delta e(t_z)$ is the nucleon polarization charge.

The reduced transition probability is defined as [20]

$$B(EJ) = \frac{|M(EJ)|^2}{2J_i + 1} \tag{12}$$

## 3. Results and Discussion

Shell model calculations are performed with NuShellX [22] with the *sd* model space for neutron number ($N$) $\leq 20$, which covered the orbits $1d_{5/2}$, $2s_{1/2}$ and $1d_{3/2}$ and *sdpf* model space for $N > 20$. Results based on the *sd*-shell interactions USDB (universal *sd*-shell interaction B) for *sd*-shell model space [23] and the *sdpf* interaction sdpf-u [24] for *sdpf* model space with valence (active) protons are restricted to the *sd* shell and $N$-20 neutrons to the *pf* shell. The 20 neutrons are frozen in *s*, *p* and *sd*-shells (full *sd* valence space for *Z*-8 protons and full *fp* valence space for *N*-20 neutrons).

The radial wave functions for the single-particle matrix elements were calculated with the harmonic oscillator (HO) potential with size parameters calculated for each isotope with mass number *A* as [12]

$$b = \sqrt{\frac{\hbar}{M_p \omega}}, \quad \text{with} \quad \hbar\omega = 45A^{-1/3} - 25A^{-2/3}.$$

Microscopic perturbed calculations have been performed for *sd*-shell nuclei to include configurations excluded by the model space which incorporate one-particle-one-hole excitation from the core and the model space orbits into all higher orbits with $2\hbar\omega$ excitation. For $N > 20$, *sdpf* model space is used with average effective charges obtained from *sd*-shell model space for $T_i \neq 0$. Calculations for the reduced transition probabilities using effective charges deduced from core-polarization (CP) effects are presented for the transition $0^+ \rightarrow 2_1^+$ ($B(E2)_{CP}$) in Si, S and Ar isotopes and compared with the available experimental data give in Ref. [1]. Evidence on the coupling of the particle motion to the high-frequency quadrupole modes is provided by the $E2$ effective charge for low-energy transitions [25]. They formulated an expression for the effective charges to explicitly include neutron excess via

$$e^{\text{eff}}(t_z) = e(t_z) + e\delta e(t_z), \quad \delta e(t_z) = Z/A - 0.32(N - Z)/A - 2t_z[0.32 - 0.3(N - Z)/A].$$

Calculations of $B(E2)$ are also presented using these effective charges ($B(E2)_{B-M}$) for a comparison. Calculation of the reduced quadrupole deformation parameter is also presented for the isotopes considered in this work, which is defined as [5].

$$\beta_2 = 4\pi \left[ B(E2); 0_1^+ \rightarrow 2_1^+ \right]^{1/2} / \left( Z R_0^2 e \right), \quad \text{where } R_0 = 1.2A^{1/3}$$

### 3.1. $_{14}$Si isotopes

Reduced transition probabilities in units of $e^2$ fm$^4$ are calculated for Silicon Si isotopes ($Z=14$) with mass number $A= 26, 28, 30, 32, 34, 36, 38, 40, 42$ and with neutron number $N= 12, 14, 16, 18, 20, 22, 24, 26, 28$, respectively. The results of the $B(E2)_{CP}$ and $B(E2)_{B-M}$ are displayed in Table-1 and plotted in Figure-1.a as a function of $N$ and $A$ in comparison with the experimental values. Experimental

values are available for $^{34-42}$Si [26]. The $B(E2)_{CP}$ values are very well explained for $A$ = 28, 30, 34-42. For $^{26}$Si, the calculated value underestimates the data by about a factor of 1.7. For $A$ = 32, the calculated value of $B(E2)_{CP}$ slightly overestimates the measured value. Calculation of $B(E2)$ with B-M effective charges for $N < 20$, agree only with the measured value of $N$ =12 ($A$=26). For $N \geq 20$, The $B(E2)_{B-M}$ values, agree very well with the measured values and are close to our results. There are similarities in the behavior of the calculated and measured $B(E2)$ values as a function of mass number $A$, for $A$ = 28 to $A$ = 38.

Calculations of the excitation energies are compared with the experimental values and tabulated in Table-1 and plotted in Figure-1.b which shows a reasonable agreement except for the $^{34}$Si isotope, where the theoretical value overestimates the experimental one by about a factor of 1.6. The experimental value for $^{42}$Si is taken from Ref. [2], which provides evidence for the disappearance of $N$ = 28 spherical closure. Figure-2 shows the level scheme of the $2_1^+$ states of Si isotopes.

The minimum value for the $B(E2)$ value is obtained for $A$ = 34 ($N$ =20) as shown in Figure-1.a which corresponds to the maximum excitation energy Figure-1.b, which confirms the magic property. For the magic number $N$ = 28 ($A$ = 42), the $B(E2)$ value is higher than those of $N \geq 20$, which corresponds to a minimum value of the excitation energy. This indicates the collapse of the $N$ = 28 shell closure. If the last eight neutrons in $^{42}$Si fill the $f_{7/2}$ orbit, i.e. separating the $f_{7/2}$ –orbit from the $pf$ shells, the results of the $B(E2)$ and $E_x$ are 169 $e^2$fm$^4$ and 6.193 MeV, respectively. These results are close to those of $N$ =20 which indicate the occurrence of the magicity at $N$=28. However, configuration- mixing shell model predicts the erosion of the $N$ = 28 magicity in the neutron rich $^{42}$Si$_{28}$ isotope, which is confirmed experimentally. Collective behavior is gradually developed in neutron-rich isotopes between $N$ = 20 and $N$ = 28, where the reduced quadrupole deformation parameter is increased reaching a maximum at $N$ = 28 and then decreased, as shown in Figure-3a. The results show a rapid deformation development of Si isotopes from $N$ = 24 to $N$ = 28.

### 3.2. $_{16}$S isotopes

Reduced transition probabilities are calculated for S isotopes with mass number $A$ = 30, 32, 34, 36, 38, 40, 42, 44, 46 and with neutron number $N$ = 14, 16, 18, 20, 22, 24, 26, 28, 30, respectively. The results of the $B(E2)_{CP}$ and $B(E2)_{B-M}$ are displayed in Table-2 and plotted in Figure-4.a as a function of $N$ and $A$ in comparison with the experimental values. Our $B(E2)$ values underestimate the measured values for $N < 20$, and explain very well the measured values for $N \geq 20$. The $B(E2)$ values calculated with B-M effective charges agree very well with the measured values for all S-isotpes considered in this work, as shown in Figure-4.a.

Good agreement is obtained between the theoretical and experimental energy levels of the $2^+$ states for all S isotopes considered in this work as shown in Table-2 and Figure-4.b. Figure-5 shows the level scheme of the $2_1^+$ states of S isotopes.

The Calculated $B(E2)$ values show a decrease in quadrupole deformation with increasing neutron number, for $N \geq 14$, reaching a minimum value at $N$ = 20 ($^{36}$S), and starts to increase reaching a maximum value at $N$ = 26 ($^{42}$S). Collective behavior is gradually developed in neutron-rich isotopes between $N$ = 20 and $N$ = 26. Deformations of nuclei near $^{44}$S are larger than in $^{44}$S Figure-3b.

### 3.7. $_{18}$Ar isotopes

Reduced transition probabilities are calculated for Ar isotopes with mass number $A$= 34, 36, 38, 40, 42, 44, 46, 48 and with neutron number $N$= 16, 18, 20, 22, 24, 26, 28, 30, respectively. The results of the $B(E2)_{CP}$ and $B(E2)_{B-M}$ are displayed in Table-3 and plotted in Figure-6.a as a function of $N$ and $A$ in comparison with the experimental values. Our results agree with the experimental results of Ref. [1] for $N$ = 16 ($A$ = 34), $N$ = 20, ($A$ = 38), $N$= 26 ($A$ = 44) and $N$ = 30 ($A$ = 48). Other experimental values for $A$ = 36, 40 and 42 are underestimated, while for $N$ = 28 ($A$ = 46), the experimental value of Ref. [1] is underestimated. All the experimental $B(E2)$ values are very well explained with the B-M effective charges, except for $N$ = 22 ($A$ = 40) and $N$ = 28 ($A$ = 46). The $B(E2)$ value for $N$ = 28 tabulated in Ref. 1, is 196 $e^2$fm$^4$, which is far away from our prediction. From this low value one would expect a persisting $N$ = 28 shell gap. Recent Lifetime measurements of excited states in neutron-rich $^{44,46}$Ar [6] showed that $B(E2)$= 570 (+335,-160) $e^2fm^4$. Our calculated value is within this measured value, which shows a systematic increase in the $B(E2)$ for $N \geq 20$. This value contradicts the enhancement of the $2^+$ energy, which provides a robust evidence for the persistence of $N$ = 28 shell gap. Ebata et al. [9] have tested the low-lying strengths of $^{46}$Ar and found to be less than 200 $e^2fm^4$, which support the smaller value of $B(E2)$ reported by Coulomb excitation. However, shell model calculations predict the

breakdown of $N = 28$ as a magic number. Fair agreement is obtained between the theoretical and experimental energy levels of the $2^+$ states for all Ar isotopes considered in this work, as shown in Figure-6.b. Figure-7 shows the level scheme of the $2_1^+$ states of Ar isotopes. Mengoni *et al*. [6] showed that a slight renormalization of the B-M effective charges by 1.14 was introduced to have the results reproduce the $B(E2)$ value of semi magic $^{38}Ar_{20}$ . Shell model calculations shows maximum deformation for $N = 28$ ($A = 46$) Figure-3c, which indicates a collapse of $N = 28$ shell closure, but this value contradicts the large value of $E_x(2^+)$ in comparison with those of the adjacent isotopes.

**4. Conclusions**

Shell model calculation is adopted to calculate $E2$ transition rates of even-even Si, S and Ar isotopes including core-polarization effects through microscopic perturbed calculations which incorporate one-particle-one-hole excitation from the core and the model space orbits into all higher orbits with $2\hbar\omega$ excitation. Full *sd* valence space is used for Z-8 protons and full *pf* valence space for $N$-20 neutrons. The proton and neutron isovector effective charges as deduced from core-polarization calculations are close to each other for all isotopes considered in this work, and the $B(E2)$ values can be described by taking the average isovector effective charges $e_\pi = 1.19e$, $e_v = 0.47e$ and average isoscalar effective charges $e_\pi = 1.33e$, $e_v = 0.33e$ . Calculations of transition rates for Si, S and Ar isotopes provide insight into the evolution of shell structure and deformation in this region. Collective behavior is gradually developed in neutron-rich isotopes between $N = 20$ and $N = 28$, and the shell gap at $N = 28$ is eroded for Si isotope. The results show a systematic increase in the $B(E2)$ values for $20 \leq N \leq 28$. Shell model calculation of $B(E2)$ value predicts the collapse of $N = 28$ shell closure in Ar isotiope, which contradicts the large value of excitation energy.

**References:**

1. S. Raman, C. W. Nestor, Jr., and P. Tikkanen. **2001**. *Atomic Data and Nuclear Data Tables*, 78, pp:1-128.
2. B. Bastin,S. Gre´vy, D. Sohler, O. Sorlin, Zs. Dombra´di, N. L. Achouri, J. C. Ange´lique, F. Azaiez, D. Baiborodin, R. Borcea, C. Bourgeois, A. Buta, A. Bu¨rger, R. Chapman, J. C. Dalouzy, Z. Dlouhy, A. Drouard, Z. Elekes, S. Franchoo, S. Iacob, B. Laurent, M. Lazar, X. Liang, E. Lie´nard, J. Mrazek,  L. Nalpas, F. Negoita, N. A. Orr, Y. Penionzhkevich, Zs. Podolya´k, F. Pougheon, P. Roussel-Chomaz, M. G. Saint-Laurent, M. Stanoiu and I. Stefan. **2007**. Collapse of the N =28 Shell Closure in $^{42}$Si. *Physical Review Letters,* 99(022503).
3. H. Scheit, T. Glasmacher, B. A. Brown, J. A. Brown, P. D. Cottle, P. G. Hansen, R. Harkewicz, M. Hellström, R. W. Ibbotson, J. K. Jewell, K. W. Kemper, D. J. Morrissey, M. Steiner, P. Thirolf, and M. Thoennessen. **1996**. The Neutron-Rich Sulfur Isotopes. *Physical Review Letters*, 77, p:3967.
4. D. Sohler, Z. Dombradi, J. Timar, O. Sorlin, F. Azaiez. **2002**. Shape evolution in heavy sulfur isotopes and erosion of the N=28 shell closure. *Physical Review C*, 66(054302).
5. T. Glasmacher, B.A. Brown, M.J. Chromik, P.D. Cottle, M. Fauerbach, R.W. Ibbotson, K.W. Kemper, D.J. Morrissey, H. Scheit, D.W. Sklenick, M. Steiner. **1997**. Collectivity in $^{44}$S. *Physical Review Letters B* , 395, pp:163-168.
6. D. Mengoni, J.J. Valiente-Dobon, A. Gadea, S. Lunardi, S.M. Lenzi, R. Broda  , A. Dewald, T. Pissulla, L.J. Angus, S. Aydin D. Bazzacco , G. Benzoni (INFN, Milan) , P.G. Bizzeti, A.M. Bizzeti-Sona, P. Boutachkov, L. Corradi, F. Crespi, G. de Angelis, E. Farnea, E. Fioretto. **2010**. Lifetime measurements of excited states in neutron-rich $^{44,46}$Ar populated via a multinucleon transfer reaction. *Physical Review C*, 82(024308).
7. A. Gade, D. Bazin, C. M. Campbell, J. A. Church, D. C. Dinca, J. Enders, T. Glasmacher,  Z. Hu, K. W. Kemper, W. F. Mueller, H. Olliver, B. C. Perry, L. A. Riley, B. T. Roeder, B. M. Sherrill and J. R. Terry. **2003**. Detailed experimental study on intermediate-energy Coulomb excitation of $^{46}$Ar. *Physical Review C*, 68(014302).
8. Kazunari Kaneko, Yang Sun, Takahiro Mizusaki Hasegawa. **2011**. Shell-model study for neutron-rich *sd*-shell nuclei. *Physical Review C*, 83(014320).
9. Shwichiro Ebata, Masaaki Kimura. **2015**. Low-lying $2^+$ states generated by pn-quadrupole correlation and N =28 shell quenching. *Physical Review C*, 91(014309).
10. Z. Meisel, S. George, S. Ahn, J. Browne, D. Bazin, B. A. Brown, J. F. Carpino, H. Chung, R. H. Cyburt, A. Estradé, M. Famiano, A. Gade, C. Langer, M. Matoš, W. Mittig, F. Montes, D. J.

  Morrissey, J. Pereira, H. Schatz, J. Schatz, M. Scott, D. Shapira, K. Smith, J. Stevens, W. Tan, O. Tarasov, S. Towers, K. Wimmer, J. R. Winkelbauer, J. Yurkon, and R. G. T. Zegers. **2015**. Mass Measurements Demonstrate a Strong $N = 28$ Shell Gap in Argon. *Physical Review C*, 114(022501).

**11.** V. R. Brown, V. A. Modsen. **1975**. Core polarization in inelastic scattering and effective charges. *Physical Review C*, 11, p:1298.

**12.** Brown, B. A., Radhi R. Wildenthal B. H. **1983**. Electric Quadrupole and Hexadecupole Nuclear Excitations from the Perspectives of Electron Scattering and Modern Shell-Model Theory. *Physics Reports,* 101, p: 313.

**13.** H. Sagawa, B. A. Brown.**1984**. E2 core polarization for sd-shell single-particle states calculated with a skyrme-type interaction. *Nuclear Physics A,* 430, pp:84-98.

**14.** B. A. Brown, B.H. Wildenthal, C.F. Williamson, F.N. Rad, S. Kowalski, H. Crannell, J.T. O'Brien. **1985**. Shell-model analysis of high-resolution data for elastic and inelastic electron scattering on $^{19}$F. *Physical Review C*, 32, p:1127.

**15.** Joseph N. Ginocchio, P. Van Isacker. **1986**. Determination of the neutron and proton effective charges in the quadrupole operator of nuclear collective models**.** *Physical Review C,* 33, p:365.

**16.** M. Carchidi, B. H. Wildenthal, B. A. Brown.**1986**. Quadruple moments of *sd*-shell nuclei. *Physical Review C*, 34, p:2280.

**17.** B. A. Brown, B. H. Wildental. **1988**. Status of the nuclear shell model. *Annual Reviews Nuclear Particle Science*, 38, pp:29-66.

**18.** W. A. Richter, S. Mkhize, B. Alex Brown. **2008**. *sd*-shell observables for the USDA and USDB Hamiltonians. *Physical Review C*, 78(064302).

**19.** R. A. Radhi, E. A. Salman. **2008**. Collective E2 transitions in $^{18}$O. *Nuclear Physics A*, 806, pp:179-190.

**20.** Brussaard, P. J. GlaudemansP. W. M. **1977**. *Shell Model Applications in Nuclear Spectroscopy*. Amsterdam, NorthHoland.

**21.** Berstch, G., Borysowicz J., McManus H. Love W. G. **1977**. Interactions for inelastic scattering derived from realistic potentials. *Nuclear Physics A*, 284, p: 399.

**22.** B. A. Brown, W. D. M. Rae. **2014**. The Shell-Model Code NuShellX@MSU. *Nuclear Data Sheet*, 120, pp:115-118.

**23.** B. Alex Brown, W. A. Richter. **2006**. New "USD" Hamiltonians for the *sd* shell. *Physical Review C*, 74(034315).

**24.** F. Nowacki, A. Poves. **2009**. New effective interaction for $0\hbar\omega$ shell-model calculations in the *sd−pf* valence space. *Physical Review C*, 79(014310).

**25.** A. Bohr, B. R. Mottelson.**1975**. *Nuclear Structure*. Benjamin, New York, 2, p:515.

**26.** Andrew Ratkiewicz. **2011**. Collectivity of exotic Silicon isotopes. Ph. D dissertation, Michigan State University.

**27.** R. Winkler, A. Gade, T. Baugher, D. Bazin, B. A. Brown, T. Glasmacher, G. F. Grinyer, R. Meharchand, S. McDaniel, A. Ratkiewicz, and D. Weisshaar. **2012**. Quadrupole Collectivity beyond N = 28: Intermediate-Energy Coulomb Excitation of $^{47,48}$Ar. *Physical Review Letters*, 108, p:182501.

**Table 1-** Reduced transition probabilities in units of $e^2\,fm^4$ and excitation energies for Si isotopes ($Z = 14$). Experimental $E_x$ and B($E2$) are taken from Ref's. [1, 2, 26].

| $A$ $_{14}$Si | $(E_x)_{theo.}$(MeV) | $(E_x)_{exp.}$(MeV) | $e_\pi$ , $e_v$ | $B(E2)_{CP}$ | $e_\pi$ , $e_v$ B-M | $B(E2)_{B-M}$ | $B(E2)_{exp.}$ |
|---|---|---|---|---|---|---|---|
| 26 | 1.897 | 1.796 | 1.19, 0.48 | 207 | 1.22, 0.91 | 377 | 356±34 |
| 28 | 1.932 | 1.779 | 0.34, 0.34 | 353 | 1.18, 0.82 | 500 | 326±12 |
| 30 | 2.265 | 2.235 | 1.21, 0.46 | 207 | 1.15, 0.75 | 282 | 215±10 |
| 32 | 2.053 | 1.941 | 1.19, 0.48 | 192 | 1.12, 0.68 | 231 | 113±33 |
| 34 | 5.245 | 3.327 | 1.2, 0.46 | 138 | 1.09, 0.62 | 114 | 85±33 $95^{+19}_{-18\,(b)}$ |
| 36 | 1.723 | 1.399 | 1.11, 0.22 | 105 | 1.06, 0.57 | 200 | 190±60 $219^{+47}_{-37\,(b)}$ |
| 38 | 1.395 | 1.084 | 1.22, 0.35 | 216 | 1.04, 0.53 | 277 | 190±70 $259^{+67}_{-46\,(b)}$ |
| 40 | 1.217 | 0.9[a] | 1.23, 0.37 | 324 | 1.02, 0.48 | 350 | $309^{+19}_{-66\,(b)}$ |
| 42 | 1.124 | 0.77[a] | 1.26, 0.37 | 409 | 1.01, 0.45 | 381 | 404±107 [b] |
| 44 | 1.342 | | 1.24,0 .41 | 292 | 0.99, 0.41 | 234 | |

**(a)**      **Ref. [2]**
**(b)**      **Ref. [26]**
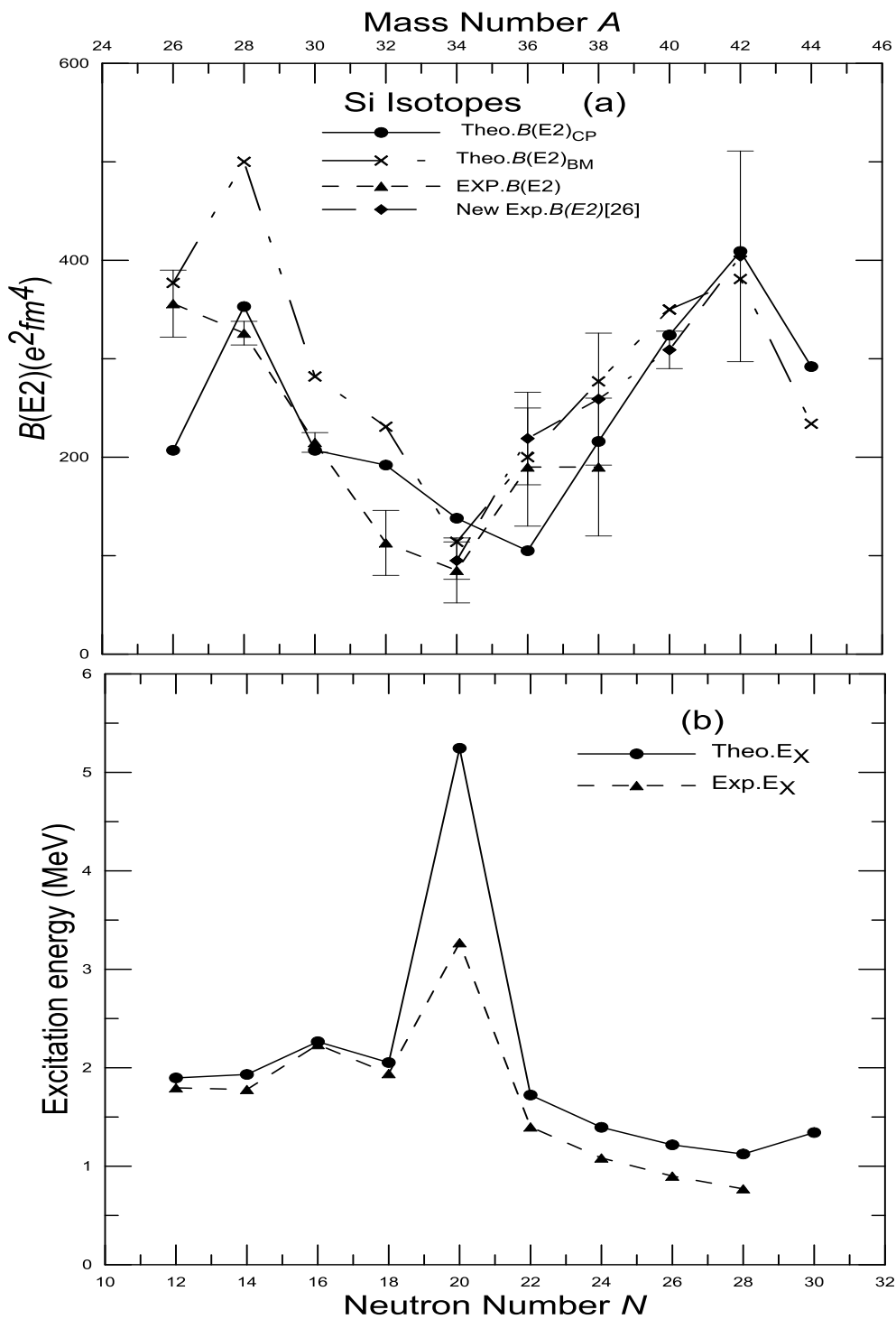
**Figure 1-** Calculated and measured $B(E2; 0^+ \rightarrow 2^+)$ and excitation energy of eve- even Si isotopes. The experimental values are taken from Ref's. [1, 2, 26].
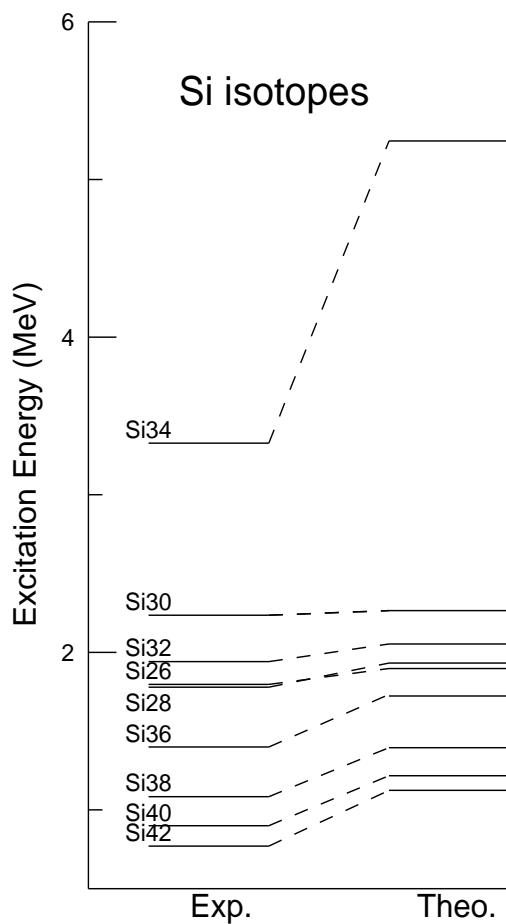
**Figure 2-** The calculated and measured excitation energies for 2$^+$ states of eve- even Si isotopes. The experimental values are taken from Ref's. [1, 2].
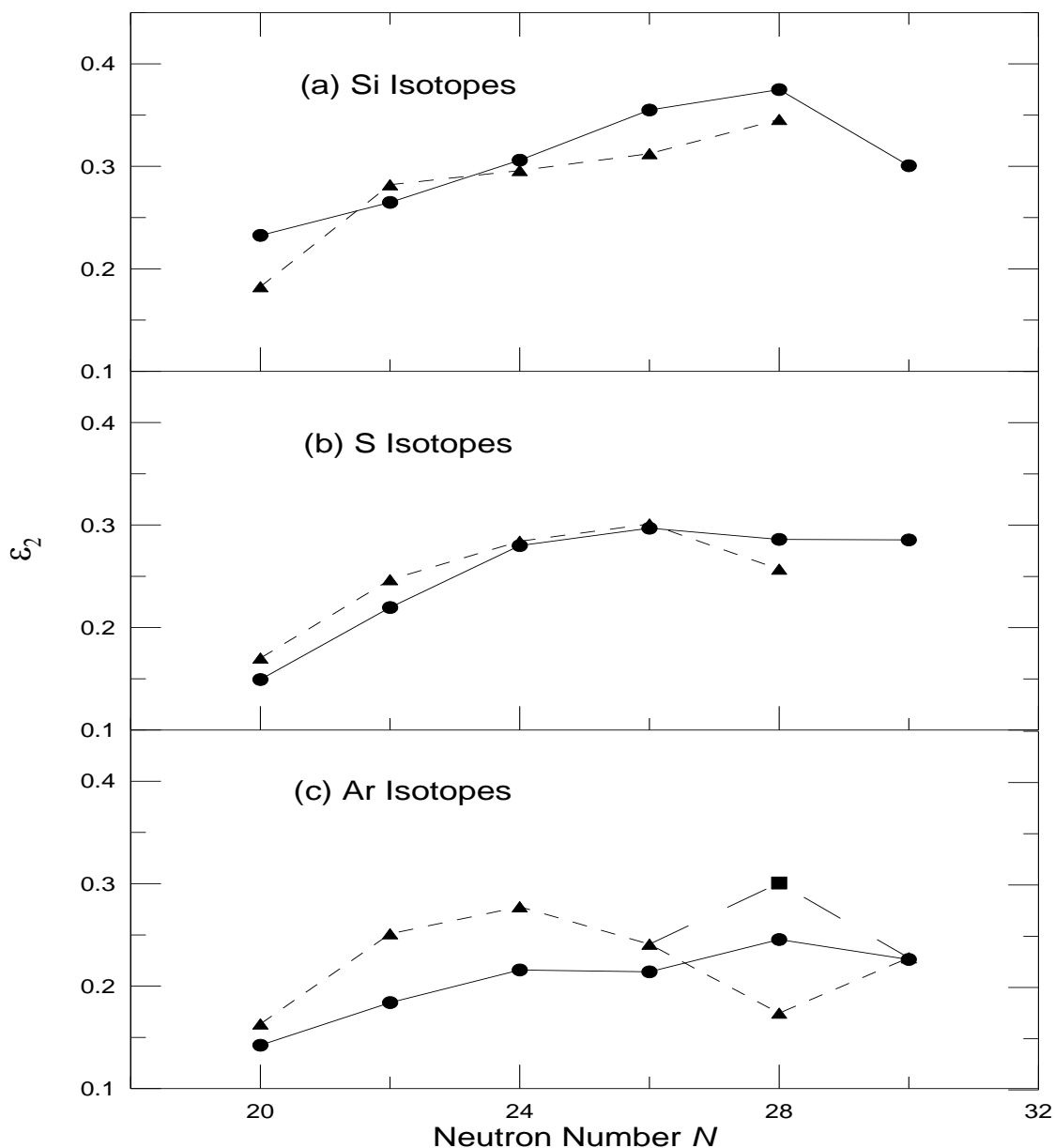
**Figure 3-** Reduced deformation parameter $\beta_2(\varepsilon_2)$ for Si (a), S (b) and Ar (c) isotopes. Theoretical values are represented by solid line and solid circles. Experimental values deduced from Re. [1] are represented by Dashed line and solid triangles. Experimental value deduced from Ref. [6] is represented by Solid Square.

**Table 2-** Reduced transition probabilities in units of $e^2 \, fm^4$ and excitation energies for S isotopes (Z=16). Experimental $E_x$ and $B(E2)$ are taken from Ref. [1].

| $A$ $_{16}$S | $(E_x)_{thor.}$(MeV) | $(E_x)_{exp.}$(MeV) | $e_\pi$, $e_\nu$ | $B(E2)_{CP}$ | $e_\pi$, $e_\nu$ B-M | $B(E2)_{B\text{-}M}$ | $B(E2)_{exp.}$ |
|---|---|---|---|---|---|---|---|
| 30 | 2.265 | 2.210 | 1.21, 0.46 | 251 | 1.21, 0.89 | 373 | 324±41 |
| 32 | 2.160 | 2.230 | 0.32, 0.32 | 209 | 1.18, 0.82 | 336 | 300±13 |
| 34 | 2.131 | 2.127 | 1.17, 0.49 | 161 | 1.15, 0.75 | 221 | 212±12 |
| 36 | 3.382 | 3.290 | 1.17, 0.42 | 80 | 1.12, 0.7 | 73 | 104±28 |
| 38 | 1.459 | 1.292 | 1.25, 0.32 | 153 | 1.1, 0.64 | 236 | 235±30 |
| 40 | 0.942 | 0.900 | 1.25, 0.33 | 264 | 1.08, 0.6 | 385 | 334±36 |
| 42 | 0.999 | 0.890 | 1.28, 0.33 | 334 | 1.06, 0.53 | 408 | 400±60 |
| 44 | 1.171 | 1.315 | 1.27, 0.36 | 348 | 1.04, 0.51 | 369 | 310±90 |
| 46 | 1.183 | | 1.27, 0.35 | 348 | 1.02  0.48 | 357 | |
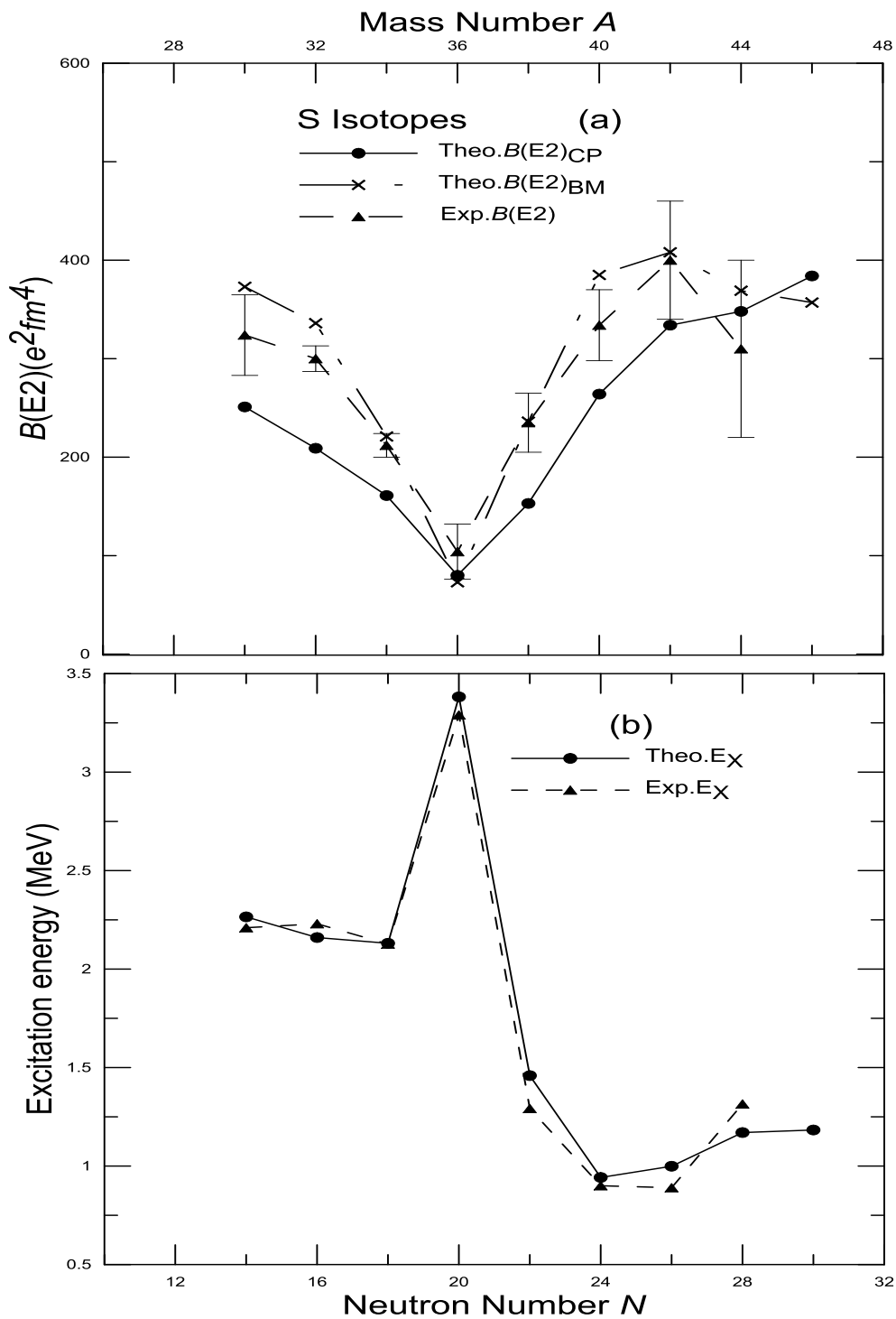
**Figure 4-** Calculated and measured $B(E2; 0^+ \rightarrow 2^+)$ and excitation energy of eve- even S isotopes. The experimental values are taken from Ref. [1].
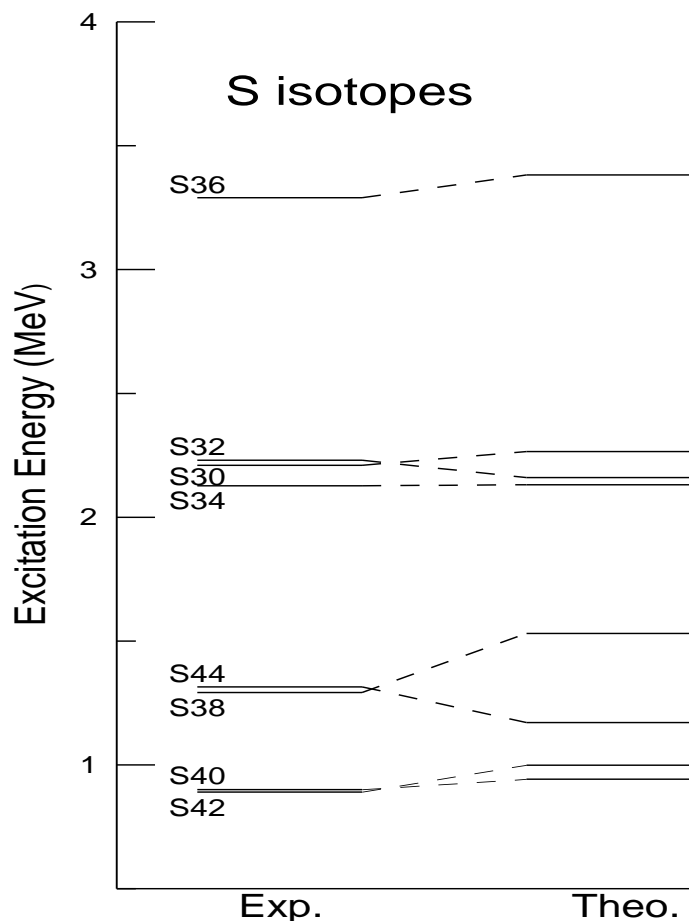
**Figure 5-** The calculated and measured excitation energies for $2^+$ states of eve- even S isotopes. The experimental values are taken from Ref. [1].

**Table 3-** Reduced transition probabilities in units of $e^2fm^4$ and excitation energies for Ar isotopes ($Z$=18). Experimental $E_x$ and B($E2$) are taken from Ref's. [1, 6, 27].

| $A$ $_{18}$Ar | $(E_x)_{thor.}$(MeV) | $(E_x)_{exp.}$(MeV) | $e_\pi$ , $e_\nu$ | $B(E2)_{CP}$ | $e_\pi$ , $e_\nu$ B-M | $B(E2)_{B-M}$ | $B(E2)_{exp.}$ |
|---|---|---|---|---|---|---|---|
| 34 | 2.131 | 2.090 | 1.17, 0.49 | 191 | 1.21, 0.89 | 282 | 240±40 |
| 36 | 1.818 | 1.970 | 0.33, 0.33 | 224 | 1.18, 0.82 | 324 | 300±30 |
| 38 | 1.844 | 2.167 | 1.2, 0.47 | 99 | 1.15, 0.76 | 155 | 130±10 |
| 40 | 1.281 | 1.460 | 1.28, 0.28 | 138 | 1.13, 0.71 | 245 | 330±40 |
| 42 | 1.155 | 1.208 | 1.19, 0.48 | 260 | 1.11, 0.66 | 353 | 430±100 |
| 44 | 1.087 | 1.144 | 1.19, 0.48 | 272 | 1.09, 0.62 | 359 | 345±41 335+22[a] -90 |
| 46 | 1.594 | 1.550 | 1.19, 0.48 | 380 | 1.07,0.58 | 528 | 196±39 570+335[a] -160 |
| 48 | 1.192 | 1.0[b] | 1.19, 0.48 | 341 | 1.05, 0.54 | 460 | 346±55[b] |

**(a)**      **Ref. [6]**
**(b)**      **Ref. [27]**
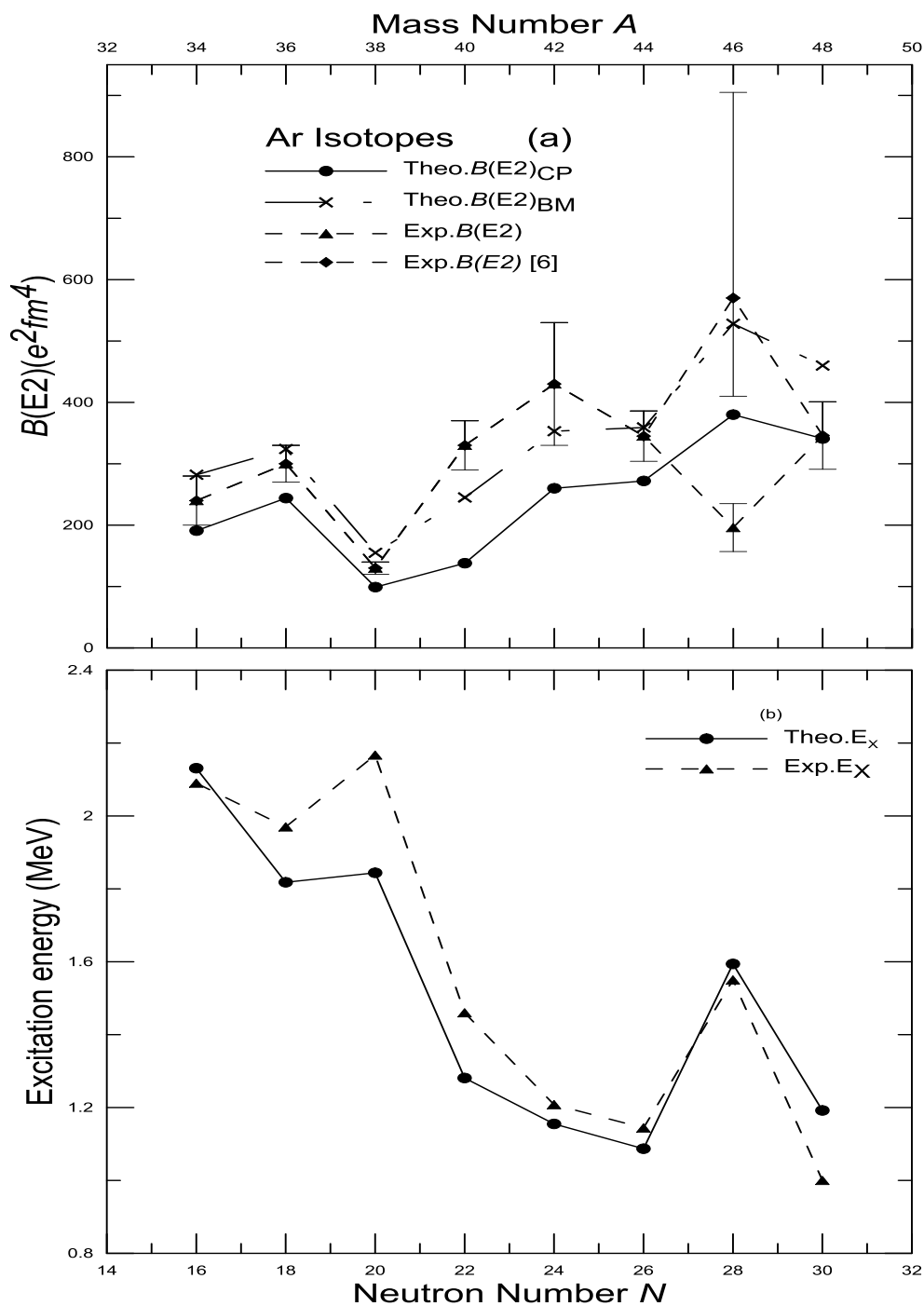
**Figure 6-** Calculated and measured $B(E2; 0^+ \rightarrow 2^+)$ and excitation energy of eve- even Arisotopes. The experimental value for $A= 46$ ($N= 28$) is taken from Ref. [6] and for $A= 48$ ($N= 30$) are taken from Ref. [27].
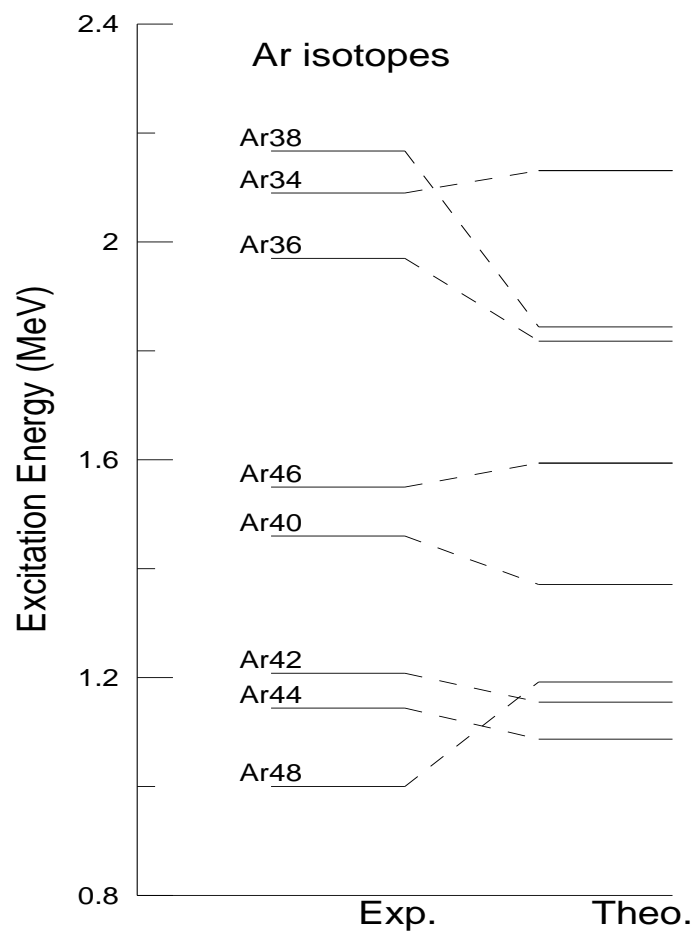
**Figure 7-** The calculated and measured excitation energies for $2^+$ states of eve- even Ar isotopes. The experimental values are taken from Ref. [1].